Pressure-Enhanced Intrinsic Anomalous Hall Conductivity in the Kagome Ferrimagnet $TbMn_6Sn_6$

Hao Sun(孙浩)[1,2], Jiabin Qiao(乔佳斌)[1,2*], Weian Guo(郭维安)[3], Pengyu Zheng(郑鹏宇)[3], Yuwei Liu(刘雨微)[1,2], Pengda Ye(叶鹏达)[4,5], Yuemei Li(李月美)[1,2], Shucui Sun(孙淑翠)[6], Deng Hu(胡灯)[1,2], Yongkai Li(李永恺)[1,2], Yanpeng Qi(齐彦鹏)[7,8,9], Zhiwei Wang(王秩伟)[1,2], Meiling Jin(金美玲)[1,2*], Jie Chen(陈洁)[1,2*], Zhiping Yin(殷志平)[3,10*], and Xiang Li(李翔)[1,2*]

[1]*Centre for Quantum Physics, Key Laboratory of Advanced Optoelectronic Quantum Architecture and Measurement (MOE), School of Physics, Beijing Institute of Technology, Beijing 100081, China*
[2]*Beijing Key Laboratory of Quantum Matter State Control and Ultra-Precision Measurement Technology, School of Physics, Beijing Institute of Technology, Beijing 100081, China*
[3]*School of Physics & Astronomy and Center for Advanced Quantum Studies, Beijing Normal University, Beijing 100875, China*
[4]*Key Lab of Advanced Optoelectronic Quantum Architecture and Measurement (MOE) and School of Physics, Beijing Institute of Technology, Beijing 100081, China*
[5]*Key Laboratory of Biomimetic Robots and Systems, Ministry of Education, State Key Laboratory of Intelligent Control and Decision of Complex System, and School of Mechatronical Engineering Beijing Institute of Technology, Beijing 100081, China*
[6]*Quantum Design (Beijing) Co., Ltd., Beijing 100015, China*
[7]*State Key Laboratory of Quantum Functional Materials, School of Physical Science and Technology, ShanghaiTech University, Shanghai 201210, China*
[8]*ShanghaiTech Laboratory for Topological Physics, ShanghaiTech University, Shanghai 201210, China*
[9]*Shanghai Key Laboratory of High-resolution Electron Microscopy, ShanghaiTech University, Shanghai 201210, China*
[10]*Key Laboratory of Multiscale Spin Physics (Ministry of Education), Beijing Normal University, Beijing 100875, China*

(Received 9 December 2025; accepted manuscript online 7 January 2026)

The kagome ferrimagnet $TbMn_6Sn_6$, featuring a pristine Mn kagome lattice, has emerged as a candidate Chern magnet with a large intrinsic anomalous Hall effect (AHE). While chemical substitution can modulate its properties, hydrostatic pressure provides a disorder-free route to manipulate electronic and magnetic interactions. Herein, we investigate the effects of hydrostatic pressure on electrical and magneto-transport in $TbMn_6Sn_6$ up to 18.3 GPa. Pressure significantly enhances hysteresis in the magnetoresistance and Hall responses, causing a concurrent monotonic coercive field increase, suggesting the enhancement of interlayer magnetic couplings in a robust *c*-axis ferrimagnetic order. The intrinsic anomalous Hall conductivity increases considerably from 129.5 $S\cdot cm^{-1}$ at ambient pressure conditions to 448.7 $S\cdot cm^{-1}$ at 14.0 GPa—an enhancement of 247% that is unprecedented among pressure-tuned kagome magnets. Based on density functional theory calculations, we reveal that pressure induces multiple gap openings near the Fermi level, giving rise to pronounced Berry curvature hotspots that may contribute to the AHE. Our results show that pressure can be used to enhance the intrinsic topological responses of this kagome magnet.

DOI: 10.1088/0256-307X/43/3/030704 CSTR: 32039.14.0256-307X.43.3.030704

The kagome lattice is a two-dimensional network of corner-sharing triangles that features flat bands, Dirac points, and van Hove singularities, providing an ideal platform for exploring topological electronic states and geometrical frustration.[1–4] When magnetic atoms populate this lattice, as in recently discovered kagome metals, symmetry-protected Dirac crossings evolve into Weyl points under exchange splitting conditions, while spin-orbit coupling further generates topologically nontrivial electronic structures.[3–20] This magnetic kagome-lattice system offers a compelling platform that can be used to explore the interplay between magnetism and band topology as well as the anomalous Hall effect (AHE).[21,22]

The hexagonal RMn_6Sn_6 (R166, where R is a rare-earth element) family comprises the prototypical magnetic kagome system.[3,4,9–20] The Mn atoms form a kagome network in the basal plane of the hexagonal crystal structure [Fig. 1(a)]. Remarkably, unique crystal structures with

*Corresponding authors. Email: jiabinqiao@bit.edu.cn; jinml@bit.edu.cn; jiechen.phy@bit.edu.cn; yinzhiping@bnu.edu.cn; xiangli@bit.edu.cn
© 2026 Chinese Physical Society and IOP Publishing Ltd. All rights, including for text and data mining, AI training, and similar technologies, are reserved.

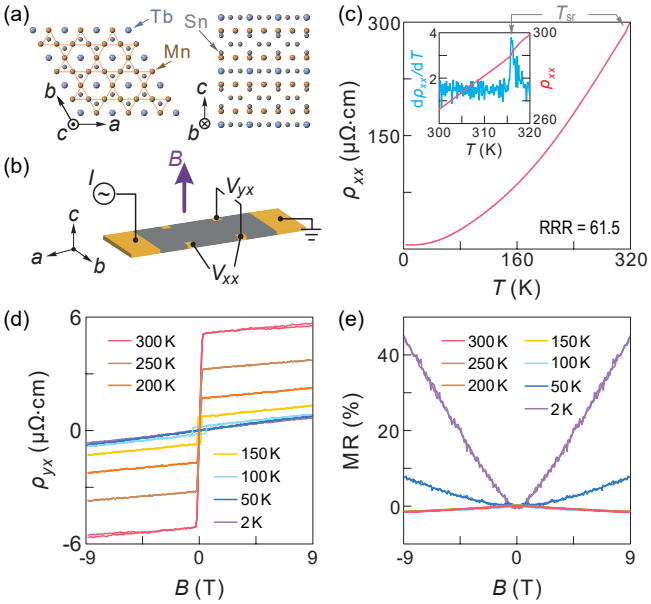

Fig. 1. (a) Schematic of top and side views of the crystal structure of $TbMn_6Sn_6$. (b) Experimental setup for electrical and magneto-transport measurements under $B \parallel c$ and ambient pressure conditions. (c) Longitudinal resistivity ρ_{xx} as a function of temperature T under ambient pressure conditions. The inset shows the T dependence of ρ_{xx} (red) and $\mathrm{d}\rho_{xx}/\mathrm{d}T$ (blue). A kink (peak) occurs in the trace of ρ_{xx} ($\mathrm{d}\rho_{xx}/\mathrm{d}T$) at $T_{\mathrm{sr}} \approx 316\,\mathrm{K}$, indicating the spin-reorientation transition. (d) Anomalous Hall resistivity ρ_{yx} as a function of magnetic field B at a set of Ts under ambient pressure conditions. (e) Field dependence of MR at a set of Ts under ambient pressure conditions.

different rare-earth elements give rise to rich magnetic phase diversity.[9–20] In this family, $TbMn_6Sn_6$ has emerged as a candidate Chern topological magnet within its quantum limit.[9] In this magnet, strong ferromagnetic coupling within the Mn kagome layers competes with the antiferromagnetic coupling in the Mn–Tb interlayer, forming a robust three-dimensional ferrimagnetic network that stabilizes both the magnetic order and topological state. Recent scanning tunneling spectroscopy studies have identified a gapped Dirac point approximately 130 meV above the Fermi level (E_{F}) in the surface band structure.[9] This Chern gap has a large Berry curvature, which is likely the dominant contributor to the intrinsic anomalous Hall conductivity (AHC) in $TbMn_6Sn_6$. However, recent studies have presented a more complex picture of the observed AHE.[23] They revealed that the AHC in $TbMn_6Sn_6$ originates from multiple contributions across the three-dimensional Brillouin zone rather than solely from a single high-symmetry point. This is further supported by the fact that the AHC is considerably enhanced in $Tb_xMg_{1-x}Mn_6Sn_6$,[24] which is associated with band structure modulation and Berry curvature accumulation caused by Mg substitution. To understand and explain this discrepancy, additional investigations of the origin of the AHE in $TbMn_6Sn_6$ are required.

In addition to chemical substitution, the application of high pressure serves as a clean, disorder-free alternative to tune the interatomic distance and modulate band structures, magnetic orders, and their interplay. Moreover, hydrostatic-pressure muon-spin rotation (μSR) measurements have recently demonstrated that the out-of-plane, topological ferrimagnetic ground state is stabilized in pressurized $TbMn_6Sn_6$.[25] This opens up opportunities to examine the effect of pressure on the electronic structures and properties of such ferrimagnets, which helps unravel the underlying mechanisms of the AHE therein.

Pressure has been employed to characterize and manipulate magnetic orders and AHE in diverse kagome magnets. For example, the AHE is suppressed monotonically upon the application of pressure in the ferromagnetic Weyl semimetal $Co_3Sn_2S_2$.[26] In the V-based kagome magnet RV_6Sn_6 (R = Gd, Tb), the pressure modulates the cooperative interaction between the V-derived kagome bands and R-layer states, effectively controlling both the magnitude and sign of the intrinsic AHC.[27] By contrast, $LiMn_6Sn_6$ exhibits remarkable robustness in terms of its structure, magnetism, and Berry curvature (up to 8.5 GPa), maintaining an intrinsic AHE with negligible pressure dependence.[28] These contrasting pressure responses observed in diverse kagome magnets highlight an unresolved issue regarding the potential for substantially enhancing the intrinsic AHC under high-pressure conditions.

In this study, we systematically investigated the electrical and magnetic properties of $TbMn_6Sn_6$ under high-pressure conditions. Upon the application of pressure, butterfly-shaped magnetoresistance (MR) occurs, and the coercive field monotonically increases, highlighting the role of pressure in tuning interlayer magnetic coupling. Importantly, a prominent pressure-enhanced intrinsic AHC is revealed, rising from $129.5\,\mathrm{S\cdot cm^{-1}}$ at ambient pressure to $448.7\,\mathrm{S\cdot cm^{-1}}$ at 14.0 GPa—the hitherto largest enhancement reported in pressurized kagome magnets. The scaling analysis further confirmed the considerable contribution of Tb-derived magnon scattering. According to our density functional theory (DFT) calculations, an enhancement

of the intrinsic AHC of this magnitude is likely due to pressure-stabilized, c-axis ferrimagnetic order and the emergence of Berry curvature hotspots near the Fermi level. Our results establish hydrostatic pressure as an efficient lever to amplify the Berry curvature, using this type of ferrimagnet as a practical testbed for pressure-controlled high-temperature topological spintronics.

Single crystals of $TbMn_6Sn_6$ were grown using the Sn self-flux method, following established protocols.[9,23] The residual Sn flux was removed by polishing the crystal surface. The single-phase nature was confirmed by powder X-ray diffraction with Cu-K_α radiation [see Fig. S1 of the Supplemental Material (SM)]. Single-crystal X-ray diffraction at room temperature verified that $TbMn_6Sn_6$ crystallizes in a layered hexagonal structure (space group $P6/mmm$) and lattice parameters $a = b = 5.5401\,(5)$ Å and $c = 9.0310\,(7)$ Å (see Table S1 in SM), which is consistent with previous reports in the literature.[9,23] The compound orders ferrimagnetically below its Curie temperature (∼420 K), with Tb magnetic moments aligned antiparallel to the ferromagnetically ordered Mn sublattice, owing to the strong Tb–Mn exchange coupling.[23,24,29,30] Upon cooling to $T_{sr} \approx 316$ K, $TbMn_6Sn_6$ underwent a magnetic transition from in-plane to out-of-plane ferrimagnetic ordering, as evidenced by the sudden increase in the field-cooled magnetic susceptibility (M) occurring at the spin-reorientation temperature [Fig. S2(a) in SM].[23,24,29,30]

Four-terminal electrical measurements were conducted on single crystals; the experimental configuration is illustrated in Fig. 1(b). The longitudinal and transverse resistivities were obtained by detecting the corresponding voltage signals V_{xx} and V_{yx}, respectively. The crystal exhibited typical metallic behavior with a high residual resistivity ratio of 61.5 [Fig. 1(c)], attesting to its high quality. The temperature-dependent longitudinal resistivity ρ_{xx} displays a kink near 316 K, corresponding to the spin reorientation transition, consistent with the characteristic temperature extracted from the $M(T)$ curve [Fig. S2(a) in SM].[23,29,30] Figures 1(d) and 1(e) shows the variation of the Hall resistivity (ρ_{yx}) and MR as a function of an external magnetic field (B) applied along the crystallographic c axis, respectively. The B dependence of ρ_{yx} exhibits similar hysteresis loops and saturation behaviors as those observed in the magnetization $M(B)$ at high temperatures ($T \geq 100$ K) [Fig. S2(b) in SM], whereas the hysteresis became unresolvable as T decreased ($T < 100$ K) [Fig. 1(d)]. In contrast, the MR measured from 2 to 300 K lacks the butterfly-shaped hysteresis observed in V-based compounds such as RV_6Sn_6 (R = Gd, Tb)[27] [Fig. 1(e)], suggesting a distinct magnetic anisotropy and spin configuration in $TbMn_6Sn_6$ compared with other kagome magnets. Additionally, we note the emergence of a positive (weakly negative) MR behavior at $T < 100$ K ($T \geq 100$ K). This observation agrees well with results reported previously.[20] Notably, the polarity reversal of the MR and the evolution of hysteresis behaviors occur at $T \approx 100$ K, suggesting a relationship between their underlying mechanisms.

Before the transport measurements under pressure conditions, we performed *in situ* high-pressure diffraction measurements on $TbMn_6Sn_6$ to examine the possible pressure-driven structural phase transitions, as shown in Fig. 2(a) [see also Fig. S3 in SM]. Structural determination

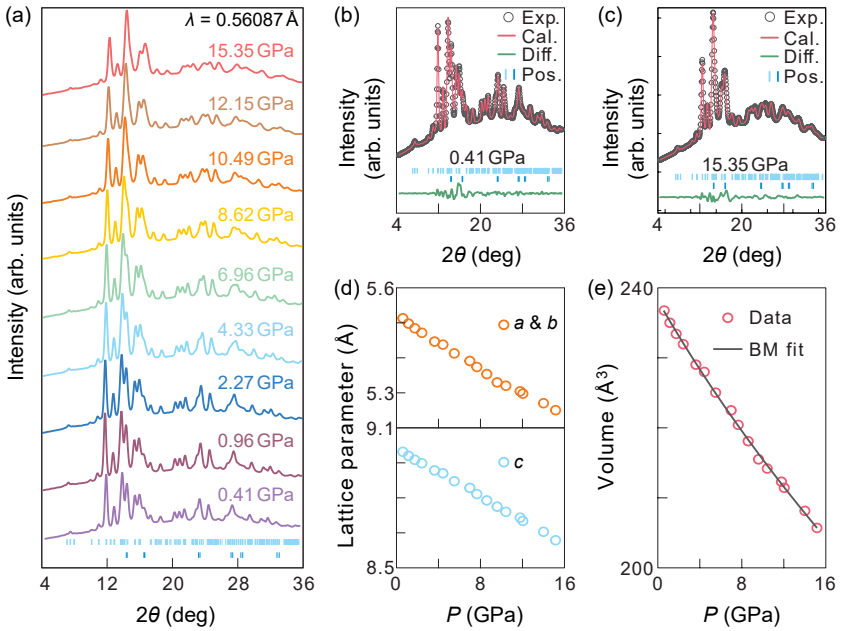

Fig. 2. (a) XRD patterns of $TbMn_6Sn_6$ at various pressures up to 15.35 GPa ($\lambda = 0.56087$ Å). (b) and (c) Rietveld refinement of the XRD profiles collected at 0.41 GPa and 15.35 GPa. Black circles and red and green curves denote the experimental data (Exp.), calculated results (Cal.), and their difference (Diff.), respectively. Light- and dark-blue vertical lines mark the Bragg peaks of $TbMn_6Sn_6$ and Pt (calibrate pressure). (d) Evolution of lattice parameters a (or b) and c versus pressure. (e) Evolution of unit-cell volume versus pressure. The data (red circles) are fitted by the third-order Birch–Murnaghan (BM) formula (black curve).

was performed using the Rietveld refinement technique using the FULLPROF SUITE software program.[31] Figures 2(b) and 2(c) shows two representative Rietveld refinement profiles at 0.41 and 15.35 GPa, respectively. The lattice parameters a (or b) and c at different pressures were extracted from the refinement, as shown in Fig. 2(d). Notably, both parameters decreased considerably and linearly at increasing pressures. Moreover, the unit-cell volume decreases at increasing pressures, as shown in Fig. 2(e). The data were fitted using the third-order Birch–Murnaghan equation of state,[32] yielding the zero-pressure volume $V_0 = 238.1\,(4)\,\text{Å}^3$, bulk modulus $B_0 = 91.6\,(\pm 4.0)$ GPa, and its first order derivative $B_0' = 2.0(\pm 0.5)$. Despite the tuning of the lattice constants, our results indicate that no structural phase transitions occur in $TbMn_6Sn_6$ and that its ferrimagnetic order (or ground state) is robust against pressures of up to approximately 15 GPa.

Electrical transport measurements under hydrostatic pressure conditions were conducted using a diamond anvil cell (DAC) with silicone oil as the pressure-transmitting medium. The experimental setup is illustrated schematically in Fig. 3(a). The temperature dependence of resistivity ρ_{xx} at various pressures is shown in Fig. 3(b) [see also Fig. S4(a) in SM]. At increasing pressures up to 18 GPa, the magnitude of ρ_{xx} decreases at $T \gtrsim 150$ K while it increases at lower temperatures. Nevertheless, the sample retains its metallic character over the entire investigated pressure range. The absence of any abrupt anomaly in ρ_{xx} at 2 K further confirms that no structural phase transition occurs at pressures up to approximately 18 GPa, consistent with the high-pressure XRD results shown above.

Hall-effect measurements were performed on the single crystal of $TbMn_6Sn_6$ under high-pressure conditions across two experimental runs (Run I: 0.5–7.3 GPa and Run II: 1.2–18.3 GPa) over a temperature range of 2–300 K [Figs. S4(b)–S4(f) and S5(a)–S5(f) in SM]. The magnetotransport behavior under high-pressure conditions deviated markedly from that under ambient conditions. Note that both the MR and Hall responses measured at 50 K [Fig. 3(c)] and 150 K [Fig. 3(d)] at 1.2 GPa exhibit distinct features compared with the features of their ambient-pressure counterparts. The anomalous Hall signal, which is weak at ambient pressure, becomes more pronounced under pressure. In addition, a butterfly-shaped MR pattern, absent at ambient pressure, emerged at high pressures and persisted throughout the investigated pressure range.

To elucidate the evolution of the Hall response with pressure, we measured the Hall resistivity ρ_{yx} at 200 K at a set of pressures, as shown in Fig. 4(a). As shown, the coercive field increases monotonically from 0.44 T at 1.2 GPa to 1.89 T at 18.3 GPa [inset of Fig. 4(a)]. This trend contrasts the pressure-induced suppression of the saturation field in TbV_6Sn_6 and parallels the behavior observed in GdV_6Sn_6.[27] Given the complex magnetic interactions and rich phase diagram of $TbMn_6Sn_6$, these unique magnetotransport behaviors are likely due to the pressure-tuned interlayer magnetic couplings. The application of high pressure can reduce the interatomic distance between the Tb and Mn layers, resulting in an enhancement of the antiferromagnetic Tb–Mn coupling and competition with the interlayer ferromagnetic Mn–Mn coupling.[24,25] The enhanced exchange couplings may further strengthen the magnetic anisotropy energy or the spin-glass clusters that act as pinning centers for the magnetic domain walls, leading to an increase in coercivity.[33,34]

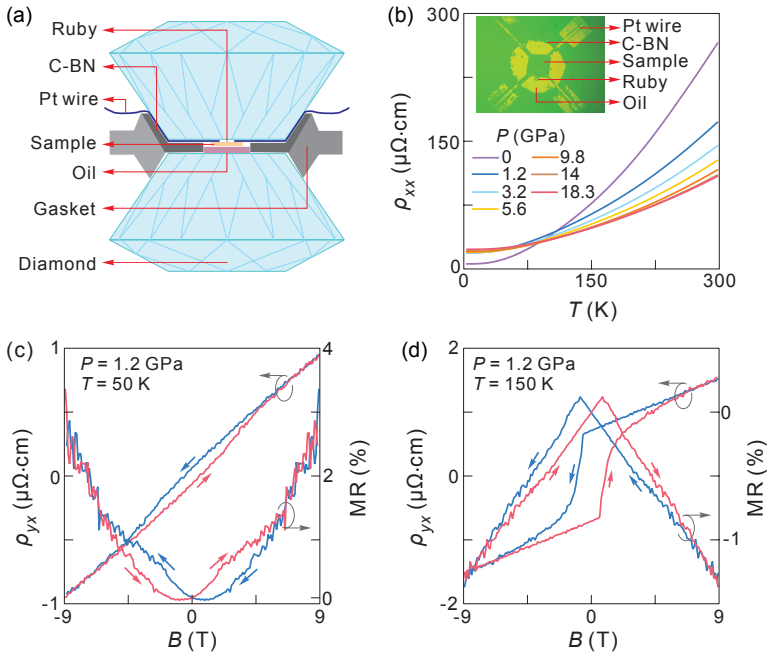

Fig. 3. (a) Schematic of the diamond anvil cell (DAC) used for high-pressure electrical measurements. (b) Longitudinal resistivity ρ_{xx} as a function of T under various pressure conditions. The inset shows an optical image of the DAC setup. (c) and (d) Hall resistivity ρ_{yx} (left) and MR (right) at 50 K and 150 K at 1.2 GPa, respectively. Red curves: −9 T to 9 T; blue curves: 9 T to −9 T.

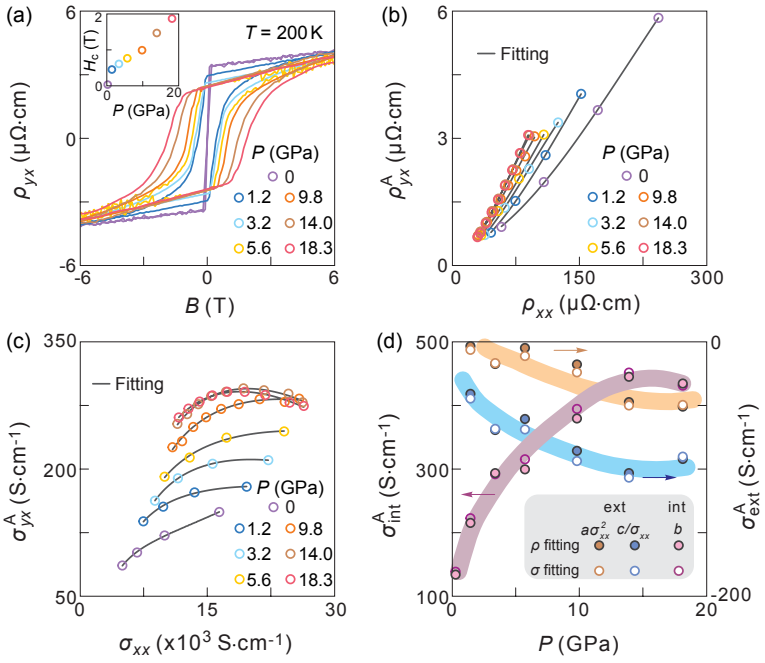

Fig. 4. (a) B dependence of the Hall resistivity ρ_{yx} at 200 K under various pressure conditions. The inset shows the pressure dependence of the coercive field H_c at 200 K. (b) Anomalous Hall resistivity ρ^A_{yx} versus ρ_{xx} recorded at T from 150 K to 300 K under various pressure conditions. The black curves are the fitted curves obtained using the relation $\rho^A_{yx} = a + b\rho^2_{xx} + c\rho^3_{xx}$. (c) Anomalous Hall conductivity σ^A_{yx} versus longitudinal conductivity σ_{xx} under various pressure conditions. The black curves are the fitted curves obtained using the relation $\sigma^A_{xy} = a\sigma^2_{xx} + b + c/\sigma_{xx}$. (d) Pressure dependence of three contributions to anomalous Hall conductivity: intrinsic term σ^A_{int} (red), extrinsic $a\sigma^2_{xx}$ term (orange), and magnon-related c/σ_{xx} term (blue). The parameters a, b, and c for two sets of data are obtained by fitting the plots of ρ^A_{yx} as a function of ρ_{xx} (ρ fitting, filled circles) and the plots of σ^A_{yx} as a function of σ_{xx} (σ fitting, empty circles).

The anomalous Hall resistivity ρ^A_{yx} was extracted from the zero-field value of ρ_{yx} by subtracting the normal linear Hall component. We then obtained the ρ^A_{yx} and corresponding longitudinal resistivity ρ_{xx} at various temperatures under distinct pressure conditions. We found that the relationship of ρ^A_{yx} with respect to ρ_{xx} under either ambient or high-pressure conditions is best described by the relation $\rho^A_{yx} = a + b\rho^2_{xx} + c\rho^3_{xx}$ [Fig. 4(b)], deviating from the standard linear-in-ρ^2_{xx} dependence [see Fig. S6 in SM]. When converting ρ^A_{yx} to the AHC σ^A_{yx} ($\approx \rho^A_{yx}/\rho^2_{xx}$) in $TbMn_6Sn_6$ where $\rho_{yx} \ll \rho_{xx}$, the variable σ^A_{yx} adheres to the relationship $\sigma^A_{yx} = a\sigma^2_{xx} + b + c/\sigma_{xx}$ [Fig. 4(c)]. These results agree with those reported in the literature,[23] where the additional c/σ_{xx} term may arise from the contribution of Tb magnons that become significant with elevated temperatures.

Furthermore, the intrinsic and extrinsic AHC values can be extracted using the ρ and σ fitting methods, as indicated in Fig. 4(d). Apparently, both the conventional extrinsic and magnon-related AHC contributions ($a\sigma^2_{xx}$ and c/σ_{xx}) are suppressed at increasing pressures. However, the intrinsic contribution exhibits a monotonic increase under pressure conditions, increasing from 129.5 S·cm^{-1} at the ambient pressure to 448.7 S·cm^{-1} at 14.0 GPa—an enhancement of 247%, which sets a record compared with respective increases on pressure-tuned kagome magnets reported previously.[26–28] These opposite responses of the intrinsic and extrinsic AHC suggest that the intrinsic AHC gradually dominates the total AHE at increasing pressures and underscores the impact of pressure on the tuning of electronic structures and intrinsic topological responses in $TbMn_6Sn_6$.

To unravel the microscopic origin of the pressure-enhanced AHC in $TbMn_6Sn_6$, we performed first-principle calculations under hydrostatic pressure conditions. Figures 5(a)–5(c) shows the electronic band structures at 6, 10, and 14 GPa, respectively. Although the characteristic kagome-derived dispersions were preserved at all pressures, the electronic structure evolved systematically through lattice compression and enhanced magnetic exchange interactions. Under increasing pressure, the Mn-derived bands broaden, and several spin orbit coupling (SOC) induced avoided band crossings-particularly near the K point and along the L–H directions-become more pronounced and shift toward the Fermi level (E_F). At $P = 6$ GPa, the band crossings near E_F remained relatively symmetric with only weak hybridization gaps, resulting in a limited Berry curvature and the smallest AHC among the studied pressures [Fig. 5(d)]. At $P = 10$ GPa, increasing the Mn–Mn hopping and exchange splitting resulted in pronounced gaps near E_F, giving rise to prominent Berry curvature hotspots. At $P = 14$ GPa, an additional gap opening emerged with multiple avoided crossings near E_F, producing the largest Berry curvature contribution of these three pressures. As there is no structural phase transition under high-pressure conditions, we first excluded the change in crystal symmetry as the origin of the observed electronic evolution. The monotonic enhancement of the intrinsic

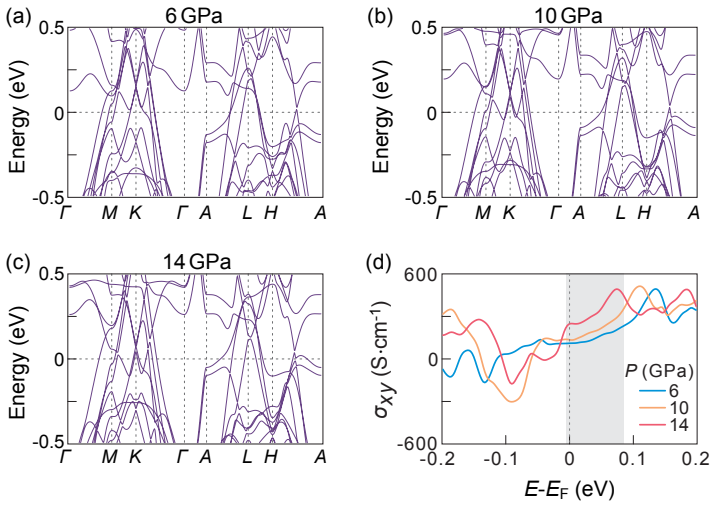

Fig. 5. (a)–(c) Band structures of $TbMn_6Sn_6$ at $P = 6$, 10, and 14 GPa. Red circles mark the gapped crossing points. (d) Energy dependence of the calculated AHC σ_{xy} at $P = 6$, 10, and 14 GPa. The shaded region marks the region wherein $\sigma_{xy}(14\,\text{GPa})>\sigma_{xy}(10\,\text{GPa})>\sigma_{xy}(6\,\text{GPa})$.

AHC with pressure near E_F may arise from the pressure-induced increment in the Berry curvature owing to gap openings and stabilization of the out-of-plane ferrimagnetic order. These results suggest that hydrostatic pressure amplifies the topological response of $TbMn_6Sn_6$ by shifting the kagome-derived avoided crossings toward E_F, thereby enhancing the intrinsic Berry-curvature mechanism underlying the AHE.

In summary, we demonstrated that hydrostatic pressure serves as an effective stimulus for enhancing the Berry curvature in the ferrimagnetic kagome metal $TbMn_6Sn_6$. High-pressure magnetotransport measurements show a record enhancement in the intrinsic anomalous Hall conductivity of 247%. We correlated this with a pressure-stabilized, out-of-plane ferrimagnetic order and the emergence of pronounced Berry curvature hotspots near the Fermi level, as revealed by first-principles calculations. These findings not only establish $TbMn_6Sn_6$ as a versatile testbed for controlling topological responses but also highlight the application of hydrostatic pressure as a disorder-free strategy for amplifying intrinsic topological properties in quantum materials.

Acknowledgements. This work was supported by the National Key R&D Program of China (Grant Nos. 2023YFA1406002 and 2020YFA0308801), the National Natural Science Foundation of China (NSFC) (Grant Nos. 12321004, 12174025, 12074041, and 12204045), the CAS Superconducting Research Project (Grant No. SCZX-0101), the Fundamental Research Funds for the Central Universities (Grant No. 2243300003), and the Innovation Program for Quantum Science and Technology (Grant No. 2021ZD0302800). This study was supported by the Synergetic Extreme Condition User Facility (SECUF) and Analysis & Testing center in Beijing Institute of Technology. Xiang Li acknowledges support from the Beijing Institute of Technology Research Fund Program (Grant No. 2023CX01027). Jiabin Qiao acknowledges support from the Beijing Institute of Technology Research Fund Program for Young Scholars. Meiling Jin acknowledges support from the Beijing Institute of Technology Laboratory Research Project (Grant No. 2023BITSYB07).

References

[1] Guo H M, and Franz M 2009 *Phys. Rev. B* **80** 113102
[2] Balents L 2010 *Nature* **464** 199
[3] Yin J X, Lian B, and Hasan M Z 2022 *Nature* **612** 647
[4] Xu X T, Yin J X, Qu Z, and Jia S 2023 *Rep. Prog. Phys.* **86** 114502
[5] Ye L, Kang M, Liu J, von Cube F, Wicker C R, Suzuki T, Jozwiak C, Bostwick A, Rotenberg E, Bell D C, Fu L, Comin R, and Checkelsky J G 2018 *Nature* **555** 638
[6] Liu E, Sun Y, Kumar N, Muechler L, Sun A, Jiao L, Yang S Y, Liu D, Liang A, Xu Q, Kroder J, Süß V, Borrmann H, Shekhar C, Wang Z, Xi C, Wang W, Schnelle W, Wirth S, Chen Y, Goennenwein S T B, and Felser C 2018 *Nat. Phys.* **14** 1125
[7] Morali N, Batabyal R, Nag P K, Liu E, Xu Q, Sun Y, Yan B, Felser C, Avraham N, and Beidenkopf H 2019 *Science* **365** 1286
[8] Yang S Y, Wang Y, Ortiz B R, Liu D, Gayles J, Derunova E, Gonzalez-Hernandez R, Šmejkal L, Chen Y, Parkin S S P, Wilson S D, Toberer E S, McQueen T, and Ali M N 2020 *Sci. Adv.* **6** eabb6003
[9] Yin J X, Ma W, Cochran T A, Xu X, Zhang S S, Tien H J, Shumiya N, Cheng G, Jiang K, Lian B, Song Z, Chang G, Belopolski I, Multer D, Litskevich M, Cheng Z J, Yang X P, Swidler B, Zhou H, Lin H, Neupert T, Wang Z, Yao N, Chang T R, Jia S, and Hasan M Z 2020 *Nature* **583** 533
[10] Chafik El Idrissi B, Venturini G, Malaman B, and Fruchart D 1991 *J. Less-Common Met.* **175** 143
[11] Clatterbuck D M and Gschneidner K A Jr 1999 *J. Magn. Magn. Mater.* **207** 78
[12] Ghimire N J, Dally R L, Poudel L, Jones D C, Michel D, Magar N T, Bleuel M, McGuire M A, Jiang J S, Mitchell J F, Lynn J W, and Mazin I I 2020 *Sci. Adv.* **6** eabe2680
[13] Chen D, Le C, Fu C, Lin H, Schnelle W, Sun Y, and Felser C 2021 *Phys. Rev. B* **103** 144410
[14] Li M, Wang Q, Wang G, Yuan Z, Song W, Lou R, Liu Z T, Huang Y, Liu Z H, Lei H, Yin Z, and Wang S 2021 *Nat. Commun.* **12** 3129

[15] Liu Z H, Zhao N, Li M, Yin Q, Wang Q, Liu Z T, Shen D, Huang Y, Lei H, Liu K, and Wang S 2021 *Phys. Rev. B* **104** 115122

[16] Pokharel G, Teicher S M L, Ortiz B R, Sarte P M, Wu G, Peng S, He J, Seshadri R, and Wilson S D 2021 *Phys. Rev. B* **104** 235139

[17] Ma W, Xu X T, Yin J X, Yang H, Zhou H, Cheng Z J, Huang Y, Qu Z, Wang F, Hasan M Z, and Jia S 2021 *Phys. Rev. Lett.* **126** 246602

[18] Gu X, Chen C, Wei W S, Gao L L, Liu J Y, Du X, Pei D, Zhou J S, Xu R Z, Yin Z X, Zhao W X, Li Y D, Jozwiak C, Bostwick A, Rotenberg E, Backes D, Veiga L S I, Dhesi S, Hesjedal T, van der Laan G, Du H F, Jiang W J, Qi Y P, Li G, Shi W J, Liu Z K, Chen Y L, and Yang L X 2022 *Phys. Rev. B* **105** 155108

[19] Lee Y, Skomski R, Wang X, Orth P P, Ren Y, Kang B, Pathak A K, Kutepov A, Harmon B N, McQueeney R J, Mazin I I, and Ke L 2023 *Phys. Rev. B* **108** 045132

[20] Gao L L, Shen S W, Wang Q, Shi W J, Zhao Y, Li C H, Cao W Z, Pei C Y, Ge J Y, Li G, Li J, Chen Y L, Yan S C, and Qi Y P 2021 *Appl. Phys. Lett.* **119** 092405

[21] Nagaosa N, Sinova J, Onoda S, MacDonald A H, and Ong N P 2010 *Rev. Mod. Phys.* **82** 1539

[22] Xiao D, Chang M C, and Niu Q 2010 *Rev. Mod. Phys.* **82** 1959

[23] Jones D C, Das S, Bhandari H, Liu X, Siegfried P E, Ghimire M P, Tsirkin S S, Mazin I I, and Ghimire N J 2024 *Phys. Rev. B* **110** 115134

[24] Wei Q, Zhou Y, Tan H, Gao L, Liu R, Jing J, Li Y, Chen D Y, Long Y Z, Li Q, Qi Y, Yan B, Teng B, and Chen D 2025 *Phys. Rev. B* **111** 064412

[25] Siegfried P E, Bhandari H, Jones D C, Ghimire M P, Dally R L, Poudel L, Bleuel M, Lynn J W, Mazin I I, and Ghimire N J 2022 *Commun. Phys.* **5** 58

[26] Liu Z Y, Zhang T, Xu S X, Yang P T, Wang Q, Lei H C, Sui Y, Uwatoko Y, Wang B S, Weng H M, Sun J P, and Cheng J G 2020 *Phys. Rev. Mater.* **4** 044203

[27] Kong X, Tao Z, Zhang R, Xia W, Chen X, Pei C, Ying T, Qi Y, Guo Y, Yang X, and Li S 2024 *Chin. Phys. Lett.* **41** 047503

[28] Gao L L, Lai J W, Chen D, Pei C Y, Wang Q, Zhao Y, Li C H, Cao W Z, Wu J F, Chen Y L, Chen X Q, Sun Y, Felser C, and Qi Y P 2024 *Chin. Phys. Lett.* **41** 057302

[29] Wenzel M, Tsirlin A A, Iakutkina O, Yin Q, Lei H C, Dressel M, and Uykur E 2022 *Phys. Rev. B* **106** L241108

[30] Li R S, Zhang T, Ma W, Xu S X, Wu Q, Yue L, Zhang S J, Liu Q M, Wang Z X, Hu T C, Zhou X Y, Wu D, Dong T, Jia S, Weng H, and Wang N L 2023 *Phys. Rev. B* **107** 045115

[31] Rodríguez-Carvajal J 1993 *Physica B* **192** 55

[32] Birch F 1947 *Phys. Rev.* **71** 809

[33] Zhang L, Huang X, Dai H, Wang M, Cheng H, Tong L, Li Z, Han X, Wang X, Ye L, and Han J 2020 *Adv. Mater.* **32** 2002032

[34] Basaran A C, Monton C, Trastoy J, Bernard R, Bouzehouane K, Villegas J E, and Schuller I K 2022 *J. Magn. Magn. Mater.* **550** 169077